A Measurement of the Relative Decay Rates of the K_2^0 Meson into its Principal Charged Modes

by **Mark Pepin**

Physical Institute of the ETH

(29. VI. 66)

Abstract. An experiment to measure the relative decay rates of the K_2^0 meson has been performed with the help of a large magnet cloud chamber placed in a nearly monochromatic beam of K_2^0 mesons. As the kinematic analysis did not allow a large fraction of the events to be identified, Monte Carlo events have been generated and used to study the recognition probabilities of events belonging to the different K_2^0 decay modes. The comparison of the Monte Carlo events to the real decays has permitted the relative decay rates of the K_2^0 meson into its principal charged modes to be evaluated via a maximum likelihood fit. The values obtained are compared to the predictions of the $|\Delta I| = 1/2$ rule.

1. Theoretical Introduction

The study of K meson decays gives some information about weak interactions involving strange particles. Comparison of the partial decay rates of different members of the isospin multiplets into corresponding decay modes allows the validity of the $|\Delta I| = 1/2$ selection rule to be tested, both in leptonic and in non-leptonic decays, while study of angular correlations in the leptonic decay modes throws some light on the nature (scalar, vector, or tensor) of the interaction between leptons and strange particles. This work is a report of the analysis of such an investigation, carried out on the K_2^0 meson[1]. Kinematic analysis alone did not allow a sufficient number of leptonic events to be unambiguously identified for a meaningful study of either angular correlations or related decay rates. However, by comparing with Monte Carlo events, we were able to estimate the relative decay rates of the K_2^0 into its principal charged decay modes and so check the $|\Delta I| = 1/2$ rule in leptonic and non-leptonic decays.

1.1 *Quantum Numbers of the K Mesons*

The phenomenon of associated production is most easily described by the introduction of a new quantum number S, called strangeness, which is taken to be conserved

---

[1] The author was mainly responsible for the analysis of the photographs and the evaluation of the results.

in strong interactions. If the strangeness of the Λ particle is by definition taken to be -1, the assignment of $S = +1$ for the K^+ and K^0 mesons, and $S = -1$ for the K^- and $\overline{K}^0$ mesons is consistent with all the observed experimental data. Conservation of isotopic spin I in strong interactions also allows the K mesons to be classified in two isospin doublets:

	I	I_3	S			I	I_3	S
K^+	$\frac{1}{2}$	$\frac{1}{2}$	1		$\overline{K}^0$	$\frac{1}{2}$	$\frac{1}{2}$	-1
K^0	$\frac{1}{2}$	$-\frac{1}{2}$	1		K^-	$\frac{1}{2}$	$-\frac{1}{2}$	-1.

The strangeness and third component of isotopic spin of a particle are not independent, but are related through the relation of Gell-Mann and Nishijima: $Q = I_3 + [B + S]/2$, where Q = charge and B = baryon number = 0 for mesons.

GELL-MANN and PAIS first pointed out [1][2]) that the neutral components K^0 and $\overline{K}^0$ of the two isotopic spin doublets do not decay independently, but are mixed by the decay Hamiltonian. There are two states of undefined strangeness, K_1^0 and K_2^0, mixtures of K^0 and $\overline{K}^0$, which diagonalize the Hamiltonian. It was thought that CP was conserved in weak interactions and that the K_1^0 and K_2^0 were CP eigenstates, with eigenvalues respectively equal to $+1$ and -1. The decay into two pions is allowed for the K_1^0, but was thought to be forbidden for the K_2^0, since a zero-charge two-pion system in the S state necessarily has CP $= +1$. The K_2^0 was therefore expected to decay predominantly through three-body modes, and consequently with a much longer lifetime. This prediction was verified by the experiment of BARDON, LANDE, LEDERMAN, and CHINOWSKY [2], which demonstrated the existence of a long-lived neutral kaon of approximately the same mass as the K_1^0, decaying into three particles, and which was identified with the K_2^0.

Recent experiments [3–6] have shown that the long-lived neutral kaon also decays into two pions, with a branching ratio of approximately 0.2%. The theoretical situation is being reconsidered, but in any case the apparent CP violation does not seem to be large enough to produce detectable effects in a measurement limited to the present experimental accuracy.

1.2 K_2^0 Decay Modes

The principal K_2^0 decay modes which have been found experimentally [7–11] are:

$$K_2^0 \to \pi^0 \, \pi^0 \, \pi^0 \tag{1}$$

$$\pi^+ \, \pi^- \, \pi^0 \tag{2}$$

$$\pi^\pm \, \mu^\mp \, \nu \tag{3}$$

$$\pi^\pm \, e^\mp \, \nu \, . \tag{4}$$

Here we have neglected the above-mentioned two-pion decay and the four-body leptonic decays $K_2^0 \to \pi^\pm \, \pi^0 \, l^\mp \, \nu$ ($l = e$ or μ) for which the predicted rates are reduced

---

[2]) Numbers in brackets refer to References, page 551.

by a factor of at least 10^3 relative to the corresponding three-body leptonic decays (3) and (4) [12]. A few events compatible with the radiative decay $K_2^0 \to \pi^+ \pi^- \gamma$ have also been found [13–15], but the branching ratio of this mode has been estimated at $\sim 1\%$ [15]. We shall assume that all decay modes not listed under (1) to (4) are negligible. This is in agreement with the known branching ratios of K^+ decay [16].

1.3 $|\Delta I| = 1/2$ Selection Rule

In non-leptonic strangeness-changing decays the rule $\Delta I_3 = \pm 1/2$ is always observed to hold. This is a consequence of the Gell-Mann and Nishijima relation, the absolute selection rules $\Delta Q = \Delta B = 0$, and the postulate $\Delta S = \pm 1$. The suggestion has been made, however, that these decays are in fact governed by the more restricting selection rule $|\Delta I| = 1/2$. This rule can be extended also to the leptonic strangeness-changing decays, if $I = 0$ is assigned to all leptons. The validity of the rule must be checked separately for non-leptonic and for leptonic decays.

The predictions of the non-leptonic $|\Delta I| = 1/2$ rule have been discussed by DALITZ [17], PAIS and TREIMAN [18], SAWYER and WALI [19], and WEINBERG [20]. Those predictions which are of interest for K_2^0 decay concern the comparison of the partial decay rates of processes (1) and (2) with those of the decays $K^+ \to \pi^+ \pi^+ \pi^-$ and $K^+ \to \pi^+ \pi^0 \pi^0$. These predictions contain corrections to allow for the phase space corresponding to the energy release of each mode. The relative phase space values are:

$$\varrho(+ + -) : \varrho(+\ 0\ 0) : \varrho(+ - 0) : \varrho(0\ 0\ 0) = 1.0 : 1.295 : 1.336 : 1.565 \,.$$

The main argument is that in the 3π decay of a K_2^0 or a K^+ alike, the final state of the π mesons is allowed to be an S-state. Because of the small energy release of these decays, this lowest possible orbital state is dominant. The spatial part of the final state wave function is therefore expected to be almost totally symmetric. This is confirmed by the fact that the Dalitz plots of these decays appear fairly uniform. It follows from Bose statistics that the isotopic spin part of the final state wave function must also be symmetric, which is possible only if $I = 1$ or $I = 3$. If S_1^0, S_3^0, S_1^+, and S_3^+ denote the amplitudes for the $I = 1$ and $I = 3$ symmetric wave functions for K_2^0 and K^+ decay, the following relations must hold [17]:

$$\frac{\Gamma(K_2^0 \to \pi^0 \pi^0 \pi^0)}{\Gamma(K_2^0 \to \pi^+ \pi^- \pi^0)} = \frac{3}{2} \frac{1.565}{1.336} \left| \frac{S_1^0 - S_3^0}{S_1^0 + 3/2\ S_3^0} \right|^2 \tag{5a}$$

$$\frac{\Gamma(K^+ \to \pi^+ \pi^0 \pi^0)}{\Gamma(K^+ \to \pi^+ \pi^+ \pi^-)} = \frac{1}{4} \frac{1.295}{1.0} \left| \frac{S_1^+ - 2\ S_3^+}{S_1^+ + 1/2\ S_3^+} \right|^2 \,. \tag{5b}$$

The $|\Delta I| = 1/2$ rule imposes $S_3^0 = S_3^+ = 0$, and so makes definite predictions for the values of these two ratios. The success of those two predictions is not a critical test of the $|\Delta I| = 1/2$ rule, however, since an $I = 3$ final state requires a $|\Delta I| = 5/2$ transition, so that only the weaker postulate $|\Delta I| \leqslant 3/2$ is proved. A more critical test of the $|\Delta I| = 1/2$ rule can be obtained by comparing the partial decay rates of the K_2^0 with those of the K^+. DALITZ [17] has shown that the ratio of all 3π modes for the K_2^0 and the K^+ is (apart from phase space corrections):

$$\frac{\Gamma(K_2^0 \to 3\pi)}{\Gamma(K^+ \to 3\pi)} = \frac{(S_1(1/2) + S_1(3/2))^2 + 3/2\ S_3(5/2)^2}{(S_1(1/2) - 1/2\ S_1(3/2))^2 + S_3(5/2)^2} \tag{6}$$

where $S_I(\Delta I)$ denotes the amplitude for a transition to a symmetrical final state of isospin I, through an interaction involving isospin change ΔI. The $|\Delta I| = 1/2$ rule predicts that the ratio on the left side of Equation (6) is equal to one. Moreover this prediction will be upset not only by the presence of an $I = 3$ final state, but also by a $|\Delta I| = 3/2$ transition leading to the $I = 1$ final state.

Equation (5a) may be used to determine how the $K_2^0 \rightarrow 3\pi$ decay rate is divided between the $\pi^0 \pi^0 \pi^0$ and $\pi^+ \pi^- \pi^0$ modes; similarly for the K^+ with Equation (5b). Phase space corrections may be introduced to obtain the $|\Delta I| = 1/2$ predictions:

$$\Gamma (K_2^0 \rightarrow \pi^+ \pi^- \pi^0) = 2 \frac{1.336}{1.295} \Gamma (K^+ \rightarrow \pi^+ \pi^0 \pi^0) \tag{7a}$$

$$\Gamma (K_2^0 \rightarrow \pi^0 \pi^0 \pi^0) = \frac{1.565}{1.0} \Gamma (K^+ \rightarrow \pi^+ \pi^+ \pi^-) - \frac{1.565}{1.295} \Gamma (K^+ \rightarrow \pi^+ \pi^0 \pi^0) . \tag{7b}$$

SAWYER and WALI [19] and WEINBERG [20] have also proposed tests of the $|\Delta I| = 1/2$ rule which are free from the assumption that the final state must be totally symmetric. If deviations from perfect symmetry exist they will produce a certain departure from a constant matrix element in the $K_2^0 \rightarrow 3\pi$ and $K^+ \rightarrow 3\pi$ decays. It has been shown [20] that if the $|\Delta I| = 1/2$ rule holds, linear relationships of the form

$$W(T) \, dT = \left(1 + \alpha \frac{T}{M_K}\right) \Phi(T) \, dT \tag{8}$$

can be expected for the energy spectra of the individual pions in these decays. Here T is the kinetic energy of the pion considered, M_K is the mass of the decaying kaon, $\Phi(T) \, dT$ is an element of phase space, and α is a numerical coefficient. Furthermore the α coefficients for the different decays are related; in particular they have the same value for the π^0 of $K_2^0 \rightarrow \pi^+ \pi^- \pi^0$ and the π^+ of $K^+ \rightarrow \pi^+ \pi^0 \pi^0$. However, consideration of the decay spectra does not provide good tests of the $|\Delta I| = 1/2$ rule if final state interactions, are solely responsible for the departure from a constant matrix element.

In leptonic decays critical tests of the $|\Delta I| = 1/2$ rule are given by the predictions [21–23]:

$$\Gamma (K_2^0 \rightarrow \pi^\pm \mu^\mp \nu) = 2 \Gamma (K^+ \rightarrow \pi^0 \mu^+ \nu) \tag{9a}$$

$$\Gamma (K_2^0 \rightarrow \pi^\pm e^\mp \nu) = 2 \Gamma (K^+ \rightarrow \pi^0 e^+ \nu) . \tag{9b}$$

In these relations the phase space corrections are negligible.

1.4 Decay Amplitude for the Leptonic Modes

If a local lepton current and the two component neutrino are assumed, the Feynman decay amplitude for the leptonic modes (3) and (4) may be written in the general form [24]:

$$M = \frac{G}{\sqrt{2}} \sum_j F_j \left(\overline{\psi}_l(p) \, O_j \, (1 + \gamma_5) \, \psi_\nu(q)\right) . \tag{10}$$

Here l is an index referring to the charged lepton (μ or e) and p and q are the 4-momenta of the charged lepton and the neutrino. The expressions F_j take account of the current of strong interactions between the kaon and the pion, with j an index referring to the scalar, vector, and tensor parts of this interaction. For Lorentz

invariance the product $F_j O_j$ must be scalar, and the ways in which this may be achieved are:

Interaction	O_j	$F_j O_j$
Scalar	1	$M_K f_S$
Vector	γ_α	$i \left(f_1 P_\alpha + f_2 Q_\alpha \right)$
Tensor	$\sigma_{\alpha\beta} = \dfrac{1}{2 i} \left(\gamma_\alpha \gamma_\beta - \gamma_\beta \gamma_\alpha \right)$	$\dfrac{i f_T}{M_K} \left(P_\alpha Q_\beta - P_\beta Q_\alpha \right) \sigma_{\alpha\beta}$.

Here P and Q are the 4-momenta of the kaon and the pion, and α and β are component indices, running from zero to three. The γ are the Dirac matrices. The form factors f_S, f_1, f_2, and f_T are real if time reversal invariance is valid; in the rest frame of the decaying kaon they are a function only of the total pion energy. If momentum and energy conservation are taken into account, and redundant angles – which only specify the orientation of the whole system – are eliminated, the final configuration of the decay may be completely specified by two independent variables, for instance Q_0 and p_0, the pion and charged lepton total energies. The transition probability dW can then be obtained from the square of the matrix element, summed over spins. If the lepton current has the same form as in the universal theory of β and μ decay [25], the interaction must be purely vector. The differential transition rate is then given by [24, 26, 27]:

$$\frac{dW}{dQ_0 \, dp_0} = \frac{G^2 f_V^2}{16 \pi^3} \left(2 M_K p_0 q_0 - M_K^2 \left(W_0 - Q_0 \right) \right.$$
$$\left. + m_l^2 \left(- 2 q_0 \left(\frac{f_2}{f_V} \right) + \left(\frac{f_2}{f_V} \right)^2 \left(W_0 - Q_0 \right) \right) \right) \tag{11}$$

where $f_V = f_1 + f_2$, $q_0 = M_K - Q_0 - p_0$, and $W_0 = (M_K^2 + m_\pi^2 - m_l^2)/2 M_K$ is the maximum pion energy; m_π and m_l are the pion and charged lepton masses. The integration of Equation (11) over p_0 can always be carried out and gives the pion energy spectrum. If the form factors are assumed constant over the relatively small range of variation of Q_0, it is also possible to integrate over Q_0 and so obtain the total transition rate. The terms containing f_2/f_V make a negligible contribution in the decay (4), since they are then multiplied by m_e^2, and the following relation holds [24, 28]:

$$\frac{\Gamma \left(K_2^0 \to \pi \pm \, \mu \mp \nu \right)}{\Gamma \left(K_2^0 \to \pi \pm \, e \mp \nu \right)} = 0.794 - 0.33 \left(\frac{f_2}{f_V} \right) + 0.075 \left(\frac{f_2}{f_V} \right)^2 . \tag{12}$$

The ratio f_2/f_V can therefore in principle be measured by determining the relative rates of decays (3) and (4), but two solutions will in general be obtained, since Equation (12) is quadratic.

2. Design of the Experiment

2.1 *Kinematic Identification of K_2^0 Decay*

The main charged decay modes (2), (3), and (4) of the K_2^0 have one common feature: they are all disintegrations into one neutral and two charged particles of opposite sign. Observation of such a decay in a magnet cloud chamber allows the momentum vectors of the two charged secondaries to be estimated through the

magnetic curvatures and initial directions of their tracks. If the incoming K_2^0 beam has been prepared so that both the magnitude and the direction of the K_2^0 momentum vector are known, the four equations expressing energy-momentum conservation in the decay still contain six independent unknowns: the masses of the three decay secondaries whose knowledge would identify the mode, and the three components of momentum of the neutral secondary. In order to identify the mode of any decay each of the possible modes must be tried out in turn, and the corresponding masses assigned to the decay products. The four equations of energy and momentum conservation then form an overdetermined system for the three components of momentum of the neutral outgoing particle. *If there were no measurement errors* such an over-determined system could only have a solution when the mass assignments are correct; if the list of possible decay modes is complete one, and only one, fit per event would then be obtained. Because of measurement errors, however, the measured decay parameters do not satisfy the overdetermined system perfectly, even when the correct mass assignments are made, and the 'goodness' of the fit obtained with each set of mass assignments must be estimated by computing the measure of the smallest corrections sufficient to ensure exact conservation of energy and momentum.

2.2   Lay-Out of the Apparatus

The experimental set-up is shown in Figure 1. A high intensity π^- beam, designed by BARBIER et al. [29], was produced on an internal Be target inside the vacuum tube

Fig. 1

Lay-out of the apparatus.

of the CERN proton synchrotron. Negative pions produced at a small forward angle were analysed in momentum by the two magnets MP1 and MP2, and a monochromatic beam was selected by the 32 mm wide momentum slit S. The accepted pions then passed through the bending magnet M102, a triplet of quadrupole lenses Q115, Q114, and Q108, and another bending magnet M108. A canal through the shielding wall between the PS tunnel and the experimental hall allowed the π^- beam to be focussed on a 2 m long cylindrical hydrogen target T H2. The entrance window of this target was made of a thickness of 3 mm of Al and 0.7 mm of Fe. Helium bags were placed in the pion beam, in order to reduce the multiple scattering. Inside the H_2 target K^0 mesons were produced through the two associated production reactions:

$$\pi^- + p \to K^0 + \Lambda^0 \tag{13}$$

$$\pi^- + p \to K^0 + \Sigma^0. \tag{14}$$
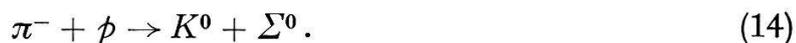
Kaons emitted forward inside a cone of 1.5° semi-angle constituted a nearly monochromatic beam whose momentum could be calculated from that of the pions through kinematic considerations. The K^0 beam successively passed through the sweeping magnet M105, which extracted the charged particles remaining in the beam, a 10 cm thick Pb filter F to convert gamma rays, and another sweeping magnet MP. The beam finally entered the magnet cloud chamber, in which K_2^0 decays could be observed. The distance from the middle of the H_2 target to the entrance of the cloud chamber was 6.5 m, and that from the gamma filter to the entrance was 2.8 m. These distances are sufficient to allow K_1^0, Λ^0, and Σ^0 particles to decay out of the beam.

The cloud chamber, a more complete description of which is published in Reference [30], has a $40 \times 60 \times 170$ cm^3 illuminated volume, and was filled with a mixture of 80% He, 20% A, and alcohol vapour at a total pressure of 820 mm Hg. It was provided with a 26 cm diameter entrance window of mylar, 0.5 mm thick. The 2 MW magnet produces a 10.7 kG magnetic field with 3% variation over the illuminated volume.

3. Calculation of the K_2^0 Momentum Spectrum

The momentum of the π^- beam was estimated by two independent measurements:

1. During the setting-up of the beam a floating wire measurement was used to set the magnet currents and the momentum slit width so that the momentum of the beam upon entering the liquid hydrogen was 1055 $\pm$ 10 MeV/c.

2. In a separate run, tracks of the pion beam were photographed in the cloud chamber. The momenta obtained through the magnetic curvatures of 79 tracks were corrected for energy losses in 7.5 additional metres of air and in the entrance window of the cloud chamber, which the pion beam now had to traverse. The mean of the distribution so obtained occurred at a higher value (1071 MeV/c) than was expected from the floating wire measurement, the spread was greater, and the distribution had a longer tail toward low momenta.

The discrepancies between the two results may be due to the fact that during the cloud chamber measurement, and in order to keep the pion beam intensity low enough to distinguish individual tracks, the internal Be target was not plunged right into the center of the proton beam, as was done during the actual experiment. The source of the pion beam was thus slightly displaced.

For further calculations it was decided to adopt for the pion spectrum a distribution of the same shape as the one obtained in the cloud chamber measurement, but displaced so that the new mean fell at 1063 MeV/c, half-way between the values obtained in the two measurements. The adopted spectrum is shown in Figure 2.
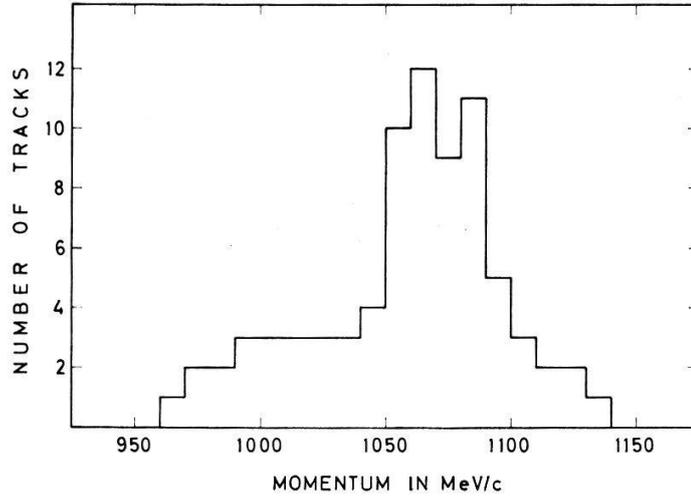
Fig. 2

Momentum spectrum of the π^- beam at target entry, obtained from the magnetic curvatures of 79 tracks and corrected to take account of the floating wire measurement.

In order to compute the momentum spectrum of K^0 mesons produced in reactions (13) and (14) by pions of this momentum distribution at target entry, we denote the mean momentum of the i-th bin by p_i, and the number of pion tracks inside this bin by N_i. It is necessary to take account of the two following facts:

1. The beam loses energy as it passes through the target, so that a pion of initial momentum p_i, interacting after having travelled the distance x inside the target, will interact at the momentum

$$p = p_i - \int_0^x \left(\frac{dp}{dx} \right) dx \cong p_i - \left(\frac{dp}{dx} \right) x$$

where (dp/dx) is the momentum loss per unit path and has the approximately constant value of 0.28 MeV/c per cm for pions around 1 GeV/c in liquid hydrogen at atmospheric pressure.

2. As it passes through the target the beam loses intensity through interactions and decays in flight. The number of pions of original momentum p_i left in the beam by the time the momentum of the survivors has decreased to p is:

$$N^{(i)}(p) = N_i \exp\left(-\int_p^{p_i} \left(n \, \sigma_{\text{tot}}(p) + \frac{1}{\lambda(p)} \right) \frac{1}{(dp/dx)} \, dp \right) \tag{15}$$

where:

n = number of protons/cm³ inside the target

$\sigma_{\text{tot}}(p)$ = total $\pi^- p$ cross section at momentum p

$\lambda(p)$ = $p \, \tau_\pi \, c/m_\pi$ = decay length for pions of momentum p.

The function $N^{(i)}(p)$ was calculated for each bin of the histogram of Figure 2. The values of $\sigma_{\text{tot}}(p)$ were taken from References [31, 32]. The number of pions of any incoming momentum which have momentum p at some point within the target is

$$N(p) = \sum_i N^{(i)}(p) \, ,$$

where the sum extends over those values of i for which $p_i - (dp/dx) L \leqslant p \leqslant p_i$ and where $L = 2$ m is the total length of the target.
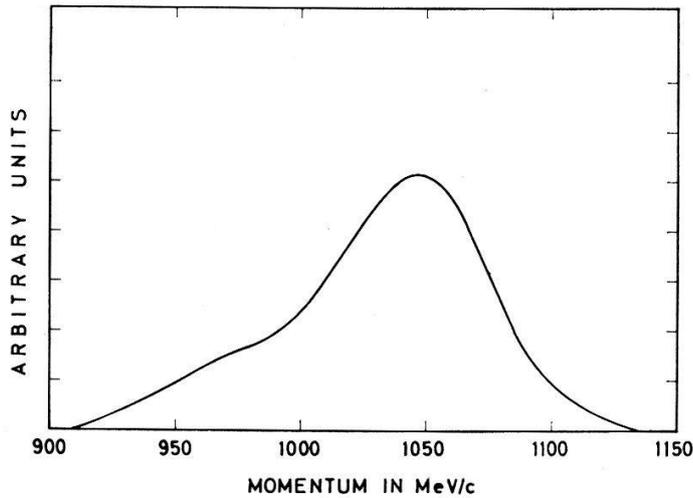
Fig. 3

Momentum spectrum of the π^- beam at interaction point, corrected to take account of beam depletion and energy losses inside the target.

This function $N(p)$ represents the pion spectrum at interaction point and is shown in Figure 3. Even if the error in the momentum of the incoming pion beam had been $\Delta p = \pm 10$ MeV/c, the spectrum at interaction point would still have had a width of 76 MeV/c; the additional 56 MeV/c error is produced by the length of the target, which cannot be reduced without diminishing the number of K_2^0's. The only two K^0-producing reactions whose thresholds fall below the upper limit of this spectrum are the afore-mentioned reactions (13) and (14), with thresholds at 897 MeV/c and 1035 MeV/c respectively. For each of these two reactions relativistic kinematics allow us to calculate the laboratory momentum $q(p)$ of a K^0 produced at 0^0 by a pion of laboratory momentum p. The spectrum $n(q)$ of kaons decaying inside the chamber is given by:

$$n(q) \propto N(p) \left(\frac{dp}{dq}\right)_{\vartheta*=0} \left(\frac{d\sigma}{d\Omega*}\right)_{\vartheta*=0} \left(\frac{d\Omega*}{d\Omega_{\text{lab}}}\right)_{\vartheta*=0} \Omega_{\text{lab}} \, P_{\text{decay}} \tag{16}$$

where

$\vartheta*$ $\quad = $ production angle in the c.m.s.

$\Omega*$ $\quad = $ solid angle in the c.m.s.

Ω_{lab} $\quad = $ solid angle in the laboratory $= 0.0022$ steradian

$(d\sigma/d\Omega*)_{\vartheta*=0}$ $\quad = $ diff. cross section in the forward direction and in the c.m.s. for the process considered

P_{decay} $= \exp(-x_1/\lambda(q)) - \exp(-x_2/\lambda(q)) =$ probability that the K_2^0 decays in the chamber

x_1 $=$ distance from middle of target to entry of chamber $= 6.5$ m

x_2 $=$ distance from middle of target to exit from chamber $= 8.2$ m

$\lambda(q)$ $= q\,\tau_K\,c/M_K =$ decay path of K_2^0 of momentum q.

The values of the differential cross section for $\Lambda^0 K^0$ production were obtained from published values [33, 34, 35] of the partial cross section for this process and from the angular distribution of CRAWFORD et al. [36]. Those for $\Sigma^0 K^0$ production were obtained from Reference [36], assuming isotropic production. The resulting momentum spectrum for the K_2^0's decaying inside the chamber is shown in Figure 4. The kaons produced in association with a Λ^0 are peaked at 630 MeV/c; those produced with a Σ^0 have a main peak at 405 MeV/c and a secondary maximum at 230 MeV/c. This is due to the fact that K^0's produced in this reaction have such a low c.m.s. velocity that those which are emitted directly backwards also go directly forward in the laboratory. This new contribution to the spectrum was calculated by a formula very similar to Equation (16), but inside which $\vartheta^* = 180°$ was substituted for $\vartheta^* = 0°$.
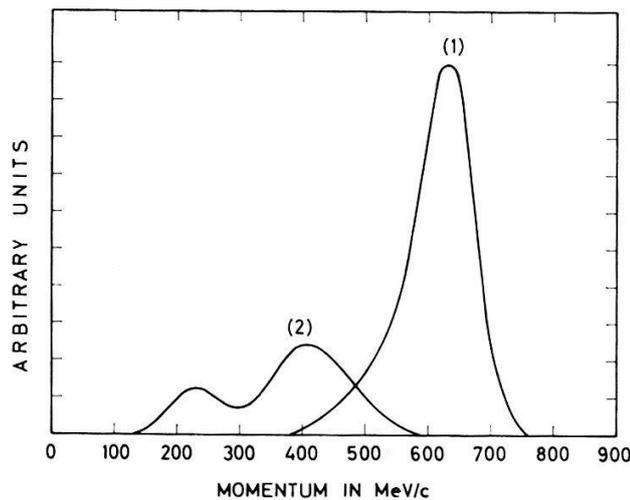
Fig. 4

Calculated momentum spectrum of the K_2^0 mesons decaying inside the cloud chamber
1) for $\Lambda^0 - K^0$ associated production; 2) for $\Sigma^0 - K^0$ associated production.

The relative abundance of decays of K_2^0 mesons produced in association with a Λ^0 or a Σ^0 was estimated from the ratio of the areas under the two curves of Figure 4 and turned out to be 0.72 to 0.28.

4. Analysis

4.1 Scanning and Measuring

In six weeks of effective running time 10000 expansions of the chamber were made at the rate of one expansion every four minutes. At each expansion the chamber was photographed by four 35 mm cameras, giving four stereoscopic views of every event.

For each portion of the chamber the scanning was done on the three best views, by a physicist and a scanner working together. Since a K_2^0 decay into any charged mode is expected to produce a V^0-type decay pattern, all events fulfilling the following conditions were logged for measurement: two tracks of opposite sign that appear to converge to one point on at least two views, while on neither view should there be a gap of more than 3 mm on the scanning table between the first droplet of each track and the presumed apex (3 mm on the scanning table is equal to approximately 5 mm in space). On none of the three views should the two tracks cross. Numerous events with both prongs of momentum lower than 50 MeV/c were recognized as electron pairs by their low ionisation and their very small opening angle; these events were discarded. In all, 1063 V^0-type events were found and logged. The three best views of every event were measured twice on the IEP digitalized measuring instruments of CERN.

4.2 Geometrical Reconstruction

The geometrical reconstruction of the two prongs of each V^0 was carried out with the CERN standard REAP and THRESH [37] programmes. Each trajectory was assumed to be a helix with a vertical axis and was defined by three parameters: curvature $1/\varrho$, angle of dip λ, and azimuthal angle at starting point φ. These parameters were adjusted so that the sum of squares of the distances from the measured points to the fitted curve was minimal. During this procedure the standard errors in the parameters of each track were calculated from the scatter of the measured points around the best fitted curve; these are the so-called internal errors.

The external errors in the parameters were given by the following formulae:

$$\left(\varDelta \frac{1}{\varrho}\right)_{\text{EXT}} = 8 f_0/(L \cos\lambda)^2$$
$$(\varDelta\lambda)_{\text{EXT}} = 6 \sqrt{\cos^2\lambda + 0.1} \; (f_0/L)$$
$$(\varDelta\varphi)_{\text{EXT}} = 4 f_0/L \cos\lambda \tag{17a}$$

and the correlation:

$$\left(\varDelta \frac{1}{\varrho} \varDelta\varphi\right)_{\text{EXT}} = - 32 f_0^2/L^3 \cos^2\lambda . \tag{17b}$$

It was assumed that no correlations exist between dip and curvature or between dip and azimuthal angle. In these formulae L is the length along which the track was measured and f_0 the error in the horizontal projection of the sagitta of the track. In practice the value $f_0 = 0.3$ mm was taken, corresponding to a maximum detectable momentum of 130 GeV/c for a track 1 m long. The formulae giving $\varDelta 1/\varrho$ and $\varDelta\varphi$ are straightforward; those for $\varDelta\lambda$ and the correlation term were obtained empirically by specialists of the CERN data handling division using artificially generated tracks.

With the help of a magnetic field map the analysis programmes then calculated the average magnetic field along each charged track and converted the curvatures into the corresponding momenta; the external errors were also increased to take account of field inhomogeneities.

In the normal measuring procedure the position of the apex of a V^0 was always recorded. When the apex was not clearly visible the apex coordinates were obtained

by extrapolating each prong of the V^0 backwards by a tangent drawn in the measured point nearest the apex, and by seeking the middle of the common perpendicular segment between these two tangents. The K_2^0 line of flight was taken to be a straight line from the centre of the hydrogen target to the apex. Errors in the angular coordinates of this direction were estimated by finding the extreme angle between the presumed K_2^0 line of fligt and a straight line from the apex to the border of the region where a K_2^0 could be produced.

4.3 *Kinematic Fitting*

The kinematic fitting was done by GRIND, a standard CERN programme written by R. BÖCK [38]. The five following processes were successively contemplated as a possible interpretation for each V^0, and the corresponding mass assignments given to the secondaries of the decay:

$$K_2^0 \rightarrow \pi^+ \, \pi^- \, \pi^0$$
$$\pi^+ \, \mu^- \, \bar{\nu}$$
$$\pi^- \, \mu^+ \, \nu$$
$$\pi^+ \, e^- \, \bar{\nu}$$
$$\pi^- \, e^+ \, \nu \; .$$

For each event this list had to be gone through twice: the first time it was assumed that the K_2^0 had been produced in association with a Λ^0, the second time, with a Σ^0. This makes ten decay hypotheses in all. From the calculations of Chapter III (see Figure 4) it was known that in the first case the magnitude of the K_2^0 momentum could be taken equal to 630 ± 48 MeV/c, where the error was chosen so as to give 67% probability that the momentum indeed falls inside this interval; this error coincides with that obtained from the half-width at $1/\sqrt{e}$ of the peak. For a K_2^0 produced in association with a Σ^0 the incoming momentum was taken equal to 405 ± 95 MeV/c. This error again gives 67% probability that the momentum falls inside this interval, but the error is now much larger than the half-width of the peak at 405 MeV/c (which would have been ± 66 MeV/c). This is due to the secondary maximum at 230 MeV/c. For simplicity it was decided to take this large error rather than go through the list of five possible interpretations a third time. Calculations inside the analysis programmes are formulated in terms of reciprocal momentum, and GRIND assumes this quantity to be normally distributed.

If the neutral incoming, positive outgoing, negative outgoing, and neutral outgoing tracks, in that order, are labelled with an index i which takes on the values from 1 to 4, the four constraint equations expressing energy and momentum conservation in any decay hypothesis will be:

$$\sum_{i=1}^{4} p_i \cos\lambda_i \cos\varphi_i = 0 \qquad \sum_{i=1}^{4} p_i \cos\lambda_i \sin\varphi_i = 0$$

$$\sum_{i=1}^{4} p_i \sin\lambda_i = 0 \qquad \sum_{i=2}^{4} \sqrt{p_i^2 + m_i^2} = \sqrt{p_1^2 + m_1^2} \qquad (18)$$

where the λ_i and φ_i are always defined so that all tracks point away from the apex. The values of p_i, λ_i, and φ_i for $i = 1$ to 3 may be considered as a vector $\boldsymbol{M}$ with nine measured components; p_4, λ_4, and φ_4 constitute a vector $\boldsymbol{M^*}$ of three unknowns.

The main task of GRIND was to find, for each decay hypothesis, the vector $\boldsymbol{M^*}$ of unknowns and a 9-dimensional vector of corrections $\boldsymbol{c}$ for the measured quantities, so that:

1. The components of the two vectors $\boldsymbol{M} + \boldsymbol{c}$ and $\boldsymbol{M^*}$ satisfy the overdetermined system (18) perfectly.

2. From the many possible values of $\boldsymbol{c}$, that one was chosen which made the function $\chi^2 = \boldsymbol{c}^T G^{-1} \boldsymbol{c}$ minimal, where G was the external error matrix for $\boldsymbol{M}$. Since no correlations between variables of different tracks were assumed, the matrix G was made up of square 3×3 submatrices along the diagonal.

The system of constraint Equations (18) is not linear, therefore all calculations inside GRIND were carried out by successive approximations.

For each event we may assume that one of the ten decay hypotheses was the correct interpretation of the event. In that case the corrected values of the measured parameters should lie close to the true values, and the χ^2 function which we have defined should indeed follow a χ^2 distribution with one degree of freedom. The probability to obtain – because of greater measurement errors – a greater χ^2 value in another observation of an identical event is given by the formula:

$$P(\chi^2) = \frac{1}{\Gamma(1/2)\ \sqrt{2}} \int\limits_{\chi^2}^{\infty} (\chi^2)^{-1/2} \exp\left(\frac{-1}{2}\ \chi^2\right) d(\chi^2) . \tag{19}$$

For each event some of the ten interpretations could be ruled out, either because the successive approximations of the fitting procedure did not converge, or because the necessary corrections were altogether too large: decay hypotheses for which $P(\chi^2) < 0.001$ were rejected. However, by routine application of all the formulae, a possible fit was in general obtained for several of the decay hypotheses. *There was no guarantee that the decay hypothesis with the largest χ^2 probability was the correct interpretation of the event.* The following remarks may be made:

1. Decays into $\pi^+\ \pi^-\ \pi^0$ were relatively easy to recognize because of the low kinetic energy release Q.

2. Because the $\pi^{\pm}\ e^{\mp}\ \nu$ decay mode has the largest Q value a certain number of events with high transverse momenta could be identified as such. Because of the large mass difference between the positive and negative secondaries it was also sometimes possible to distinguish between $\pi^+\ e^-\ \bar{\nu}$ and $\pi^-\ e^+\ \nu$.

3. No event was identified which was compatible only with $\pi^{\pm}\ \mu^{\mp}\ \nu$ decay.

4. Monte Carlo events confirm that it is difficult to identify the decay mode of a K_2^0 by kinematics alone, even when the error on the incoming K_2^0 momentum (which in our case is by far the major error) is reduced to $\pm$ 5 MeV/c.

4.4   *Rejected events*

Nine of the original 1063 events found in the scanning had one or both tracks heavily ionising (like a proton) and so could not be K_2^0 decays. They were rejected.

Of the remaining 1054 events, 257 had to be discarded because of failures in the geometrical reconstruction of the events. Each event was measured twice. Any measurement for which one or more of the following conditions were fulfilled was rejected:

1. If the geometrical reconstruction of either track failed completely. This sometimes happened for steeply dipping tracks.

2. If $(\Delta 1/\varrho)_{\mathrm{INT}} > 3 (\Delta 1/\varrho)_{\mathrm{EXT}}$: the internal error in the momentum was much larger than it was expected to be from the consideration of the maximum detectable momentum. This could happen either if the track was distorted, or through faulty measurements.

3. If $1/\varrho < 3 (\Delta 1/\varrho)_{\mathrm{EXT}}$: this meant that the track was either too short or too straight for a precise momentum determination.

4. If there was an apex reconstruction, and if the common perpendicular segment between the two extrapolating tangents was more than 3 mm long, or if the reconstructed apex was more than 2 cm away from the nearest measured point of either track. Moreover, it was checked that the reconstructed apex was located approximately where expected from looking at the event.
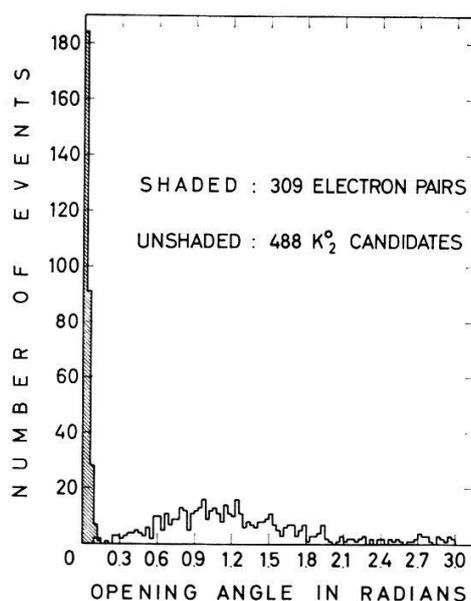
Fig. 5

Distribution of opening angles for the 797 well-reconstructed events. The 309 events compatible with $\gamma \to e^+ e^-$ are shaded. The 488 unshaded events are K_2^0 candidates.

The number of remaining events which had at least one sufficiently good measurement and reconstruction was 797. Whenever both measurements led to acceptable results the two outputs were compared to one another, and it was checked that the values obtained in both measurements were compatible, and the better one was chosen by taking account of the size of the errors and the lengths along which the tracks were measured.

This sample of 797 well-reconstructed events still contained a fairly large contamination of high-energy electron pairs. These were detected by applying the following criterion:

$$\phi - 3\,\Delta\phi \leqslant 3\,\vartheta_{\mathrm{RMS}} \qquad (20)$$

where ϕ is the measured opening angle between the two charged prongs of the V^0, $\Delta\phi$ the external error in ϕ, and ϑ_{RMS} the root mean square opening angle of an electron pair of the energy and asymmetry observed for the event. ϑ_{RMS} was calculated with the formula of M. STEARNS [39].

The histogram of opening angles for the 797 well-reconstructed events is given in Figure 5. The 309 events, which by the above criterion are compatible with electron pairs, are shaded. The 488 residual events are presumed to be K_2^0 decays. The separation is good. Further evidence for this may be obtained from Figures 6a and 6b, which represent the distribution of the height Z_{apex} of the apex above the bottom of the chamber for events respectively compatible and incompatible with electron pairs. The distribution for the 488 K_2^0 candidates is asymmetric because some events in the top half of the chamber were lost through lack of sensitivity in this region (the incoming beam was centred on $Z_{\mathrm{apex}} = 25$ cm). But the main point is that the distribution for the 309 electron pairs is very sharply peaked in the interval 20 cm $\leqslant$ $Z_{\mathrm{apex}} \leqslant 24$ cm, which contains 256 events. This is probably due to a crack in the shielding around the gamma filter. The distribution of Z_{apex} for the 488 K_2^0 candidates shows no corresponding peak, which indicates that very few electron pairs were retained in that sample. As against this, although the sample of discarded electron pairs contains 34 events with opening angles between 60 and 120 mrad, these must be true electron pairs because 27 of them are concentrated in the interval 20 cm $\leqslant$ $Z_{\mathrm{apex}} \leqslant 24$ cm.
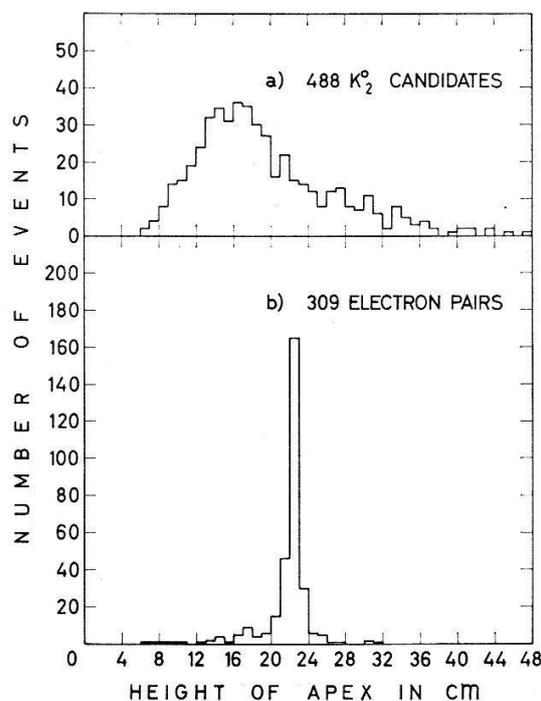
Fig. 6

Compared distributions of the height of the apex above the bottom of the cloud chamber
a) for the 488 K_2^0 candidates; b) for the 309 electron pairs.
Note the change in vertical scale.

The high contamination by electron pairs inside the 797 well-reconstructed events leads us to expect an equally high contamination in the 257 badly-reconstructed events. In fact, 141 of the 257 had very small opening angles and most probably were electron pairs. Many of them failed because of bad apex reconstructions: the two prongs of an electron pair are nearly parallel close to the apex, and the common perpendicular segment between the two extrapolating tangents is not well determined. The other 116 badly-reconstructed events had larger opening angles and were presumably K_2^0 decays. We shall examine in the next paragraph the errors which may have been introduced by their rejection.

When the kinematic fitting of the 488 well-reconstructed K_2^0 candidates had been done in GRIND, it was observed that for 48 of these events none of the ten decay hypotheses gave an acceptable fit. These events also were discarded, leaving a final sample of 440 K_2^0 decays. The possible errors introduced by their rejection will also be considered in the next paragraph.

4.5 *Background and Possible Biases*

The fairly high background of electron pairs and the method used for separating it from the K_2^0 sample have already been described.

In this experiment the background of neutron stars was quite low: approximately one star per thirty pictures. Three stars consisted of two lightly ionising prongs of opposite charge plus one short highly ionising recoil. From an analysis of stars of this type, carried out by C. VERKERK in an experiment where the neutron star background was much higher [40], we can say that the number of such stars where the recoil is so short as not to be seen is negligible.

If the non-leptonic $|\Delta I| = 1/2$ rule is valid, as seems likely, our results (see §5.5) on $K_2^0 \to \pi^+ \pi^- \pi^0$ mean that approximately 100 decays $K_2^0 \to \pi^0 \pi^0 \pi^0$ should have taken place inside the chamber. Approximately 4 Dalitz pairs should then be expected.

The programme GRIND also tested each event for kinematic compatibility with the following 2-body decays of neutral particles: $\Lambda \to p\,\pi^-$, $\bar{\Lambda} \to \bar{p}\,\pi^+$, $K_1^0 \to \pi^+ \pi^-$. Since no neutral secondaries are emitted in these decays, overconstrained fits could be obtained without feeding any information on the momentum of the decaying particle into the programme. Of the 440 accepted K_2^0 decays, 51 were also kinematically compatible with Λ decays, 47 with $\bar{\Lambda}$ decays, and 42 with K_1^0 decays. When the ionisation of the supposed proton or anti-proton was examined, and when the condition was added that the decays must take place within 5 decay lengths of the walls of the cloud chamber, no events compatible with Λ or $\bar{\Lambda}$ decays remained, and only one event compatible with $K_1^0 \to \pi^+ \pi^-$.

The 42 events kinematically compatible with K_1^0 decays may be interpreted as $K_2^0 \to \pi^+ \pi^-$, since the decay length argument is not valid for rejecting this hypothesis. The condition that the reconstructed K_2^0 direction should coincide with that of the incoming beam must now be fulfilled, however, and is sufficient to exclude this interpretation for all but two events. Since both are also compatible with normal K_2^0 decay modes, we may conclude no CP-violating effects were observed.

All events were also tested for kinematic compatibility with the following decays: $\pi^+ \to \mu^+ \nu$, $\pi^- \to \mu^- \bar{\nu}$, $K^+ \to \pi^+ \pi^0$, $K^+ \to \mu^+ \nu$, $K^- \to \pi^- \pi^0$, $K^- \to \mu^- \bar{\nu}$. Of the 440

accepted K_2^0 decays, 5 were also compatible with π^+ decays and 7 with π^- decays. A great number of events were kinematically compatible with charged kaon decays: 90 with K^+ decays and 93 with K^- decays. In 55 cases for the K^+'s, however, and in 56 for the K^-'s, the momentum of the supposed kaon was low enough to allow ionisation to give information on the decay. In every case the $K^\pm$ decay hypothesis had to be rejected. For the 72 remaining possible $K^\pm$ decays (35 of a K^+ and 37 of a K^-) a plot was made of the cosine of the angle β between the incoming K_2^0 beam and the track of the possible charged kaon. This plot is shown in Figure 7. The forward peaking is very easy to explain if these are the tracks of the decay products of forward-going K_2^0's. If the events are to be interpreted as the decays of charged kaons, the decaying particles must have been going backwards towards the apices. No reason exists for such a strong backward peaking. Accordingly these events where retained in the K_2^0 sample.
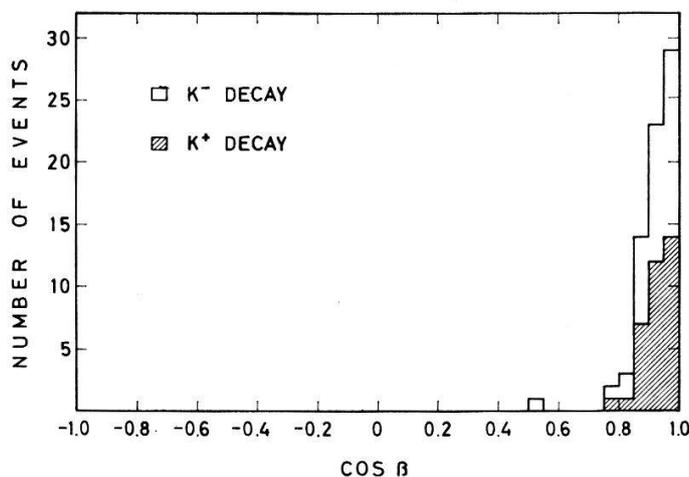
Fig. 7

Distribution of $\cos \beta$, where β is the angle between the direction of the incoming K_2^0 beam and the direction of the supposed charged kaon at the decay point, for 35 events compatible with K^+ decay (shaded) and 37 events compatible with K^- decay (unshaded).

As a further check of the background, 600 pictures were taken during the experimental run but with an empty hydrogen target. In these pictures 3 events compatible with K_2^0 decays – both kinematically and with respect to ionisation – were found. This corresponds to approximately 50 events in the 10 000 pictures of the actual experiment. These are not necessarily spurious events, but may be decays of genuine K_2^0's produced in the entrance and exit windows of the H_2-target.

We have now finished the discussion of the types of background events which may have been retained in the K_2^0 sample, and come to the events rejected during the analysis, although they may have been genuine K_2^0 decays. These events fall in two classes: 116 events whose geometrical reconstruction did not succeed, and 48 well-reconstructed events with no K_2^0 fit.

First order approximations for the geometrical parameters of 94 of the 116 badly-reconstructed events were obtained by the analysis programmes. They were used to make a plot of $p_{tr\ max}$, the transverse momentum of the secondary for which this quantity is largest; $p_{tr\ max}$ is sensitive to the energy release Q of the decay. A similar

plot was made for the 440 accepted K_2^0 decays (see Figures 8a and 8b). The distributions shown in the two histograms are well compatible up to $p_{tr\ max} = 190$ MeV/c. But whereas the distribution for the K_2^0 candidates goes down sharply after this point, the one for the badly measured events does not. We estimate that the 66 rejected events with $p_{tr\ max} \leqslant 190$ MeV/c contain the same proportions of different decay modes as the sample of 440 accepted K_2^0 decays, and that the 50 other badly-reconstructed events are mostly $\pi^\pm\,e^\mp\,\nu$ with some $\pi^\pm\,\mu^\mp\,\nu$ decays.
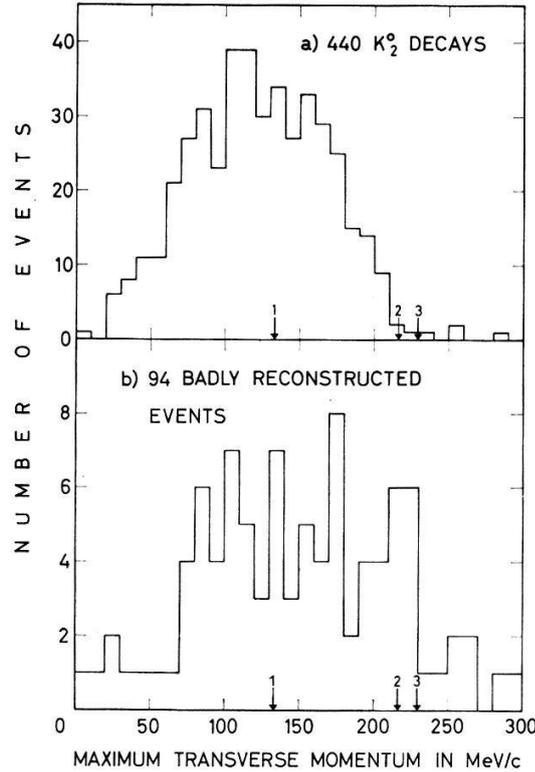
Fig. 8

Compared distributions of the maximum transverse momentum $p_{tr\ max}$
a) for the 440 accepted K_2^0 decays; b) for 94 badly-reconstructed events.
Note the change in vertical scale. The arrows marked 1, 2, and 3 indicate the extreme limit of
$p_{tr\ max}$ for $K_2^0 \to \pi^+\,\pi^-\,\pi^0$, $K_2^0 \to \pi^\pm\,\mu^\mp\,\nu$, and $K_2^0 \to \pi^\pm\,e^\mp\,\nu$ decays respectively.

The 48 well-reconstructed events which did not fit any of the ten K_2^0 decay hypotheses were analysed again, but with no constraint on the magnitude of the incoming K_2^0 momentum; 21 events then became compatible with decays of K_2^0's of low momentum. This fits in with the peak at 230 MeV/c in the K_2^0 momentum spectrum of Figure 4. The 21 fits were: $3\,\pi^+\,\pi^-\,\pi^0$ decays, $1\,\pi^+\,\mu^-\,\bar{\nu}$ decay, $8\,\pi^\pm\,e^\mp\,\nu$ decays, 9 events compatible with several types of leptonic decays. As we will see, these numbers are in good agreement with the branching ratios obtained, bearing in mind that most $\pi^\pm\,\mu^\mp\,\nu$ decays also give $\pi^\pm\,e^\mp\,\nu$ fits. Another 8 events were compatible with various background modes (kinematically and with respect to decay lengths and ionisation): 4 decays $\pi^\pm \to \mu^\pm\,\nu$, 2 decays $K^\pm \to \mu^\pm\,\nu$, 1 decay $K_1^0 \to \pi^+\,\pi^-$, 1 event with a large droplet at the apex, a possible neutron star; 19 events remained unexplained.

5. Monte Carlo Estimate of Branching Ratios

5.1 *Generation of Monte Carlo Events*

Although it was not possible to identify a large fraction of the decays, the branching ratios could still be obtained with the help of Monte Carlo events. These were used to estimate the probabilities that an event belongs to any decay hypothesis when it is known to have a given set of χ^2 values.

In all, 6000 Monte Carlo events were generated – 600 for each of the ten decay hypotheses – with the help of the programme FAKE. This programme was written at BERKELEY by G. LYNCH [41] and adapted for CERN use by C. VERKERK [42]. To generate an event according to any given decay mode a random point was chosen with a uniform distribution inside the corresponding Dalitz plot. This determined the centre-of-mass kinetic energies of two secondaries. The decay configuration was then calculated via energy and momentum conservation and the event was rotated at random in the c.m.s. so that the distribution of the normal to the decay plane became isotropic. A laboratory momentum for the K_2^0 was then chosen at random in the K_2^0 momentum spectrum used in the analysis. This means that two distributions gaussian in the reciprocal momentum, with peaks at 630 MeV/c and 405 MeV/c, were employed, *not* the three-peaked spectrum of Figure 4. For the Monte Carlo events the line of flight of the K_2^0 was always assumed to be the axis of the beam. This K_2^0 momentum was used to transform the momenta of the secondaries from c.m.s. to the laboratory. The Monte Carlo events were then distributed along the longitudinal axis of the cloud chamber according to the decay probability of a K_2^0 of the chosen momentum. The lengths of all charged tracks were obtained by calculating the trajectories the particles would have had in the magnetic field and finding the exit points from the sensitive volume.

In order that the Monte Carlo events be quite similar to the experimental ones it was still necessary to modify all the measured parameters so as to simulate the measurement errors. These parameters are the momentum, dip, and azimuthal angle of both charged secondaries, and the dip and azimuthal angle of the incoming K_2^0. The error in the magnitude of the K_2^0 momentum is already incorporated, since each event is generated with a random momentum in the spectrum, whereas in the analysis the prepared momentum is initially assumed to be either 630 MeV/c or 405 MeV/c. To simulate a measurement error a random number was chosen in a gaussian distribution with a standard deviation equal to the external error of the parameter to be modified, to which the random number was then added. For both charged tracks the external errors were determined from the track length by the formulae (17a) of §4.2. For the angular coordinates of the K_2^0 line of flight the average values of the errors found for the experimental events were used.

5.2 *Tentative Identification Procedure*

The Monte Carlo events thus generated were analysed by GRIND in exactly the same way as the experimental ones. Again each event gave as final result a set of ten χ^2 probabilities for the ten attempted fits, some of which were in general equal to zero (less than 1% of the Monte Carlo events gave no fit in all ten decay hypotheses).

By comparing the relative values of these ten probabilities for sets of events generated all according to the same decay hypothesis it was possible to discover features which characterize the events truly belonging to this decay hypothesis. In this way tentative identification procedures could be defined; the one finally retained may be defined in three steps:

1. Any event which fitted either or both of the $\pi^+ \pi^- \pi^0$ decay hypotheses (with Λ^0- or Σ^0-associated K_2^0) was ascribed to the best of these two fits, regardless of the probabilities with which the event fitted any leptonic decay hypotheses.

2. For events which fitted neither of the 3π decay hypotheses, the sum of the probabilities for the four leptonic fits of a K_2^0 produced with a Λ^0 was compared to 0.6 times the corresponding sum for the leptonic fits with Σ^0. The event was considered as a leptonic decay of a Λ^0- or a Σ^0-associated K_2^0, depending on which value was the greater. The numerical factor 0.6 is purely empirical. The need for such a factor arises from the fact that the difference of 225 MeV/c between 630 MeV/c and 405 MeV/c represents 4.7 times the standard deviation of the peak at 630 MeV/c, but only 2.4 times that of the peak at 405 MeV/c. Accordingly a genuine Λ^0-associated K_2^0 is easier to fit to a Σ^0-associated decay hypothesis than the converse.

3. Whether the event was Λ^0- or Σ^0-associated, the probabilities of the two $\pi^\pm e^\mp \nu$ fits were compared to the doubled probabilities of the two $\pi^\pm \mu^\mp \nu$ fits, and the event ascribed to whichever fit gave the greatest value. Again the factor 2 is purely empirical and compensates for the fact that a genuine $\pi^\pm \mu^\mp \nu$ decay almost always fits a $\pi^\pm e^\mp \nu$ decay hypothesis, whereas the converse is not true.

Once the tentative identification procedure was defined, the Monte Carlo events were used to determine the probabilities that an event generated according to any decay hypothesis was correctly classified by this procedure in the mode to which it belonged, or mis-classified in each of the other modes. These probabilities may be represented in a square 10×10 matrix A. The element A_{ij} in the i-th row and the j-th column is equal to the fraction of events generated according to the decay hypothesis j which were nevertheless ascribed to the hypothesis i by the tentative identification procedure. The sum of the elements of each column of the matrix A is therefore equal to unity. The greater the diagonal elements of the matrix, the more efficient is the identification. For the procedure described above the diagonal elements are approximately 0.80 for events generated according to either of the 3π hypotheses, and they are between 0.45 and 0.55 for the leptonic events.

5.3   Effects of the Transition Matrix Element

The Monte Carlo events were generated with uniform density over the Dalitz plot. As against this the experimental events are distributed over the Dalitz plot with a varying density, depending on the transition matrix element. If the outcome of the identification tests depends on the point of the Dalitz plot where the event was generated, the uniform density of the Monte Carlo events will not lead to the same matrix of classification probabilities as would be obtained with the density distribution of the real events. A matrix of classification probabilities A_{ij} valid for the experimental events may nevertheless be obtained by giving to each Monte Carlo event a

weight proportional to the density of the experimental events in the point of the Dalitz plot where it was generated. This method has the advantage of allowing the classification probabilities for the density distributions predicted by different types of interaction to be estimated simply by changing these weights.

For the final results, and in agreement with Equation (8), we weighted the Monte Carlo decays $K_2^0 \rightarrow \pi^+ \pi^- \pi^0$ with the relative transition rate $dW/d\Phi$ equal to $(1 + \alpha\, T_0/M_K)$, where T_0 is the kinetic energy of the neutral pion. The numerical value taken for α was -7.3, in agreement with previous experiments on K_2^0 decay [8, 9, 40] and in agreement also with the values obtained from the decays $K^\pm \rightarrow \pi^\pm \pi^0 \pi^0$, assuming the non-leptonic $|\varDelta I| = 1/2$ rule is valid [43].

For the leptonic decays we adopted the relative transition rate given by Equation (11) and which assumes pure vector interaction. The ratio of form factors f_2/f_V has been studied by LUERS et al. [8] – the notation used in that reference is $\xi = 1 - 2(f_2/f_V)$ – who find the two solutions $f_2/f_V \cong 0$ and $f_2/f_V \cong 3.8$. The value near zero seems more probable [8, 9] and was accordingly chosen in the estimation of the classification probabilities used for the final results.

The effect of using other transition matrix elements was also tested, however. The branching ratios are quite insensitive to these changes (see Table 3 below). This was further checked by verifying that the Monte Carlo events correctly identified by the tentative identification procedure have uniform density over the Dalitz plot. For the diagonal elements of the matrix of classification probabilities, at least, the outcome of the identification tests does not depend on the region of the Dalitz plot where the event was generated.

5.4   *Maximum Likelihood Estimation*

If the assumption is correct that the experimental events have the same classification probabilities A_{ij} as the Monte Carlo ones, the branching ratios may be obtained in the following way: let f_j $(j = 1, \ldots, 10)$ represent the true but unknown fraction of K_2^0 decays into the hypothesis j. Further, let n_i $(i = 1, \ldots, 10)$ be the number of experimental events tentatively ascribed to the i-th decay hypothesis by the identification procedure. The probability that any event of the data appears to belong to the decay hypothesis i is equal to the product of the probability that the event in reality belongs to the hypothesis j, multiplied by the probability that an event truly belonging to j appears as i; the sum over j of ten such products must then be taken:

Probability for one event $= \sum\limits_{j} f_j\, A_{ij}$.

The probability to find the set of ten values n_i that was observed is by definition called the likelihood function $\mathcal{L}$.

$$\mathcal{L} = \prod_i \left(\sum_j f_j\, A_{ij} \right)^{n_i}. \tag{21}$$

This likelihood function depends on the ten parameters f_j. By the maximum likelihood principle of statistics the best estimates of the branching ratios are those values of the f_j which make the likelihood function a maximum.

The ten parameters f_j are not all independent, but have to satisfy some constraints:

1. The sum of all the f_j must be equal to unity.
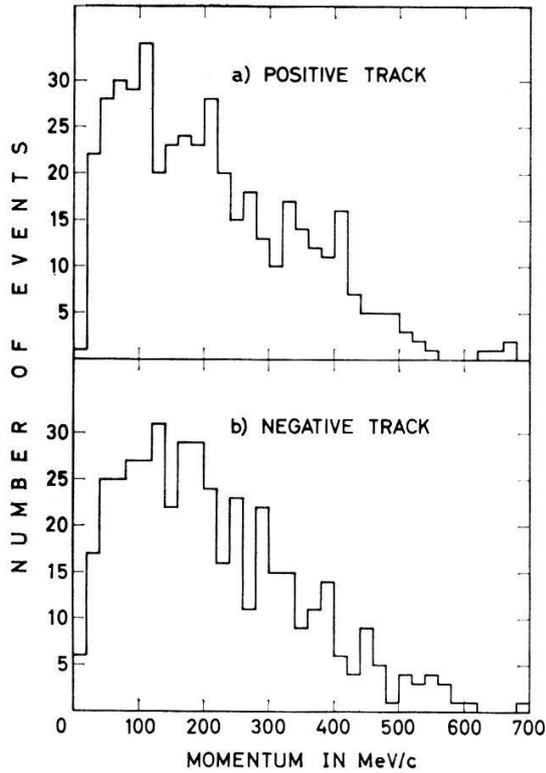
Fig. 9

Compared distributions of the momentum p. a) of the positive track; b) of the negative track for the 440 accepted K_2^0 decays.
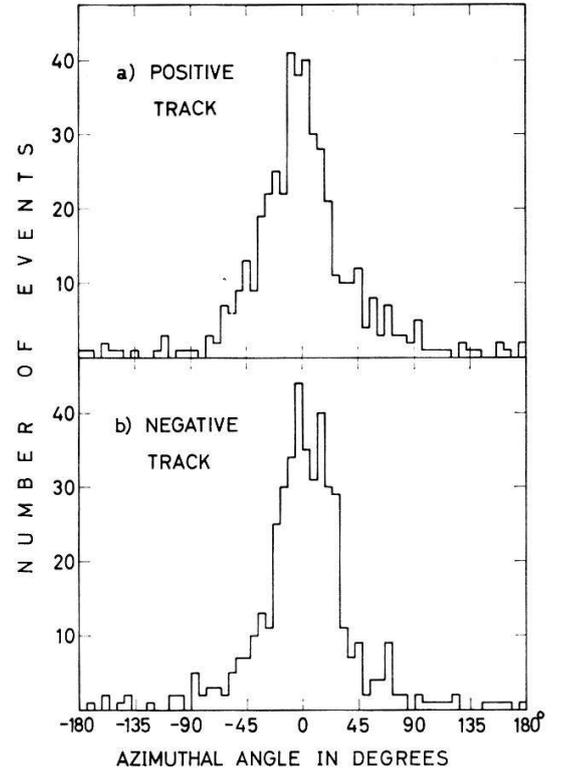
Fig. 10

Compared distributions of the azimuthal angle φ. a) of the positive track; b) of the negative track for the 440 accepted K_2^0 decays.
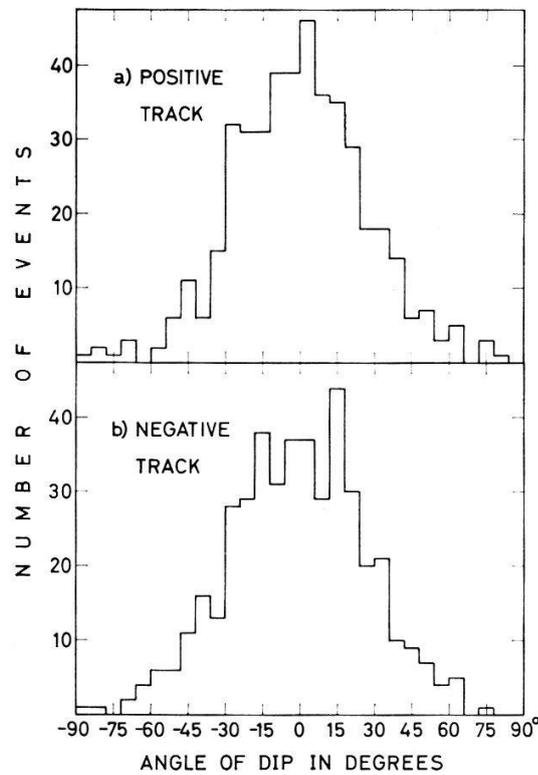
Fig. 11

Compared distributions of the angle of dip λ
a) of the positive track; b) of the negative track for the 440 accepted K_2^0 decays.

2. The relative numbers of K_2^0's decaying into $\pi^+ \pi^- \pi^0$, $\pi^\pm \mu^\mp \nu$, or $\pi^\pm e^\mp \nu$ must be the same if the K_2^0 was produced in association with either a Λ^0 or a Σ^0.
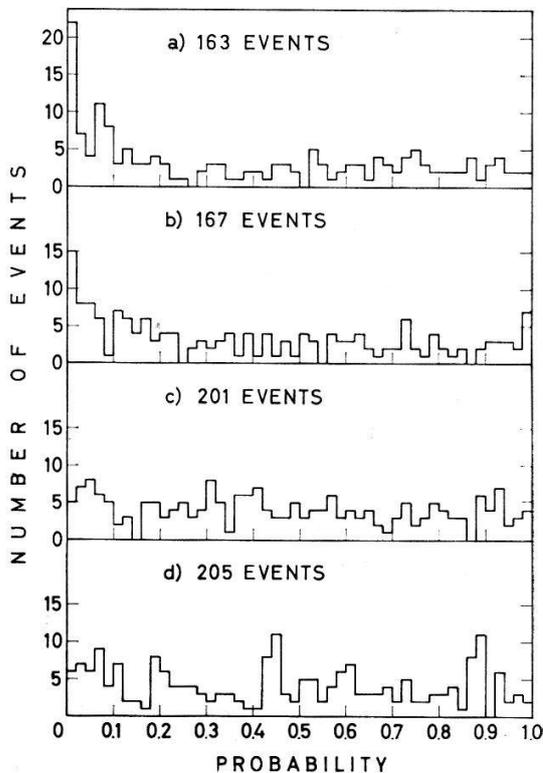
Fig. 12

Compared distributions of the probabilities assigned
a) to the fit K_2^0 (with Λ^0) $\to \pi^+ \mu^- \bar{\nu}$ for the 163 events for which this probability is > 0.001;
b) to the fit K_2^0 (with Λ^0) $\to \pi^- \mu^+ \nu$ for the 167 events for which this probability is > 0.001;
c) to the fit K_2^0 (with Σ^0) $\to \pi^+ \mu^- \bar{\nu}$ for the 201 events for which this probability is > 0.001;
d) to the fit K_2^0 (with Σ^0) $\to \pi^- \mu^+ \nu$ for the 205 events for which this probability is > 0.001.
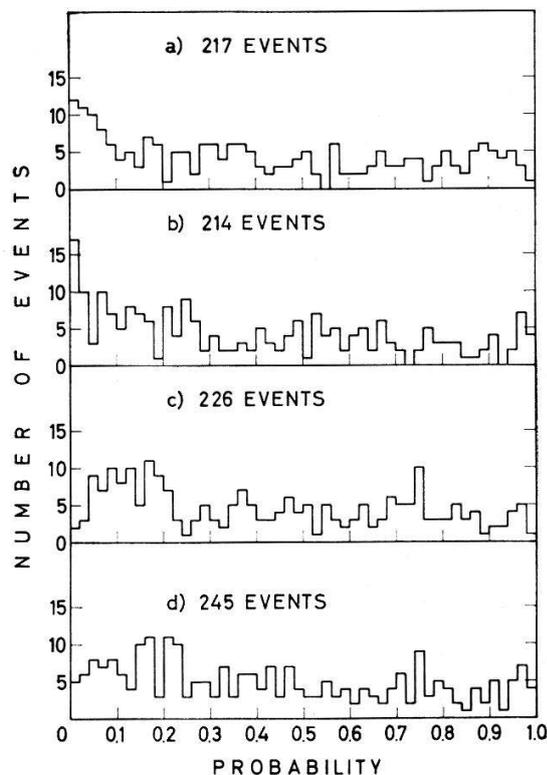
Fig. 13

Compared distributions of the probabilities assigned
a) to the fit K_2^0 (with Λ^0) $\to \pi^+ e^- \bar{\nu}$ for the 217 events for which this probability is > 0.001;
b) to the fit K_2^0 (with Λ^0) $\to \pi^- e^+ \nu$ for the 214 events for which this probability is > 0.001;
c) to the fit K_2^0 (with Σ^0) $\to \pi^+ e^- \bar{\nu}$ for the 226 events for which this probability is > 0.001;
d) to the fit K_2^0 (with Σ^0) $\to \pi^- e^+ \nu$ for the 245 events for which this probability is > 0.001.

3. No charge asymmetry was detected in the data. Figures 9, 10, and 11 show the compared distributions of p, φ, and λ for the positive and negative tracks. χ^2 tests with ten degrees of freedom were made to test the assumption that these distributions are the same, and gave respectively the values 3.1, 8.0, and 5.4. Nor was any difference detected between the distributions of the probabilities which GRIND found for charge conjugated decay modes (see Figures 12 and 13). Therefore the branching ratios for $\pi^+ \mu^- \bar{\nu}$ and $\pi^- \mu^+ \nu$ decays and for $\pi^+ e^- \bar{\nu}$ and $\pi^- e^+ \nu$ decays were constrained to be the same. This is in accordance with approximate CP conservation.

If we define the symbols b_1, b_2, b_3, and b_4:

$$b_1 = \frac{\text{No. of } \Lambda^0\text{-associated } K_2^0\text{'s}}{\text{Total no. of } K_2^0\text{'s}},$$

$$b_2 = \frac{\Gamma\left(K_2^0 \to \pi^+ \pi^- \pi^0\right)}{\Gamma\left(K_2^0 \to \text{all charged modes}\right)},$$

$$b_3 = \frac{\Gamma\left(K_2^0 \to \pi^\pm \mu^\mp \nu\right)}{\Gamma\left(K_2^0 \to \text{all charged modes}\right)},$$

$$b_4 = 1 - b_2 - b_3 = \frac{\Gamma\left(K_2^0 \to \pi^\pm e^\mp \nu\right)}{\Gamma\left(K_2^0 \to \text{all charged modes}\right)}, \tag{22}$$

the ten parameters f_j may be expressed as a function of b_1, b_2, and b_3 in the following way:

Table 1

Replacement of the 10 parameters f_j by 3 parameters b_i so as to satisfy all the constraints.

	K_2^0 produced with Λ^0	K_2^0 produced with Σ^0
$K_2^0 \to \pi^+ \pi^- \pi^0$	$f_1 = b_1 b_2$	$f_6 = (1 - b_1) b_2$
$\pi^+ \mu^- \bar{\nu}$	$f_2 = b_1 b_3/2$	$f_7 = (1 - b_1) b_3/2$
$\pi^- \mu^+ \nu$	$f_3 = b_1 b_3/2$	$f_8 = (1 - b_1) b_3/2$
$\pi^+ e^- \bar{\nu}$	$f_4 = b_1 (1 - b_2 - b_3)/2$	$f_9 = (1 - b_1) (1 - b_2 - b_3)/2$
$\pi^- e^+ \nu$	$f_5 = b_1 (1 - b_2 - b_3)/2$	$f_{10} = (1 - b_1) (1 - b_2 - b_3)/2$

These expressions for the f_j were substituted in Equation (21), which defines the likelihood function.

5.5   Results and Errors

The maximum likelihood estimates of the branching ratios b_1, b_2, and b_3 were obtained by calculating the likelihood function $\mathcal{L}$ on the points of a 3-dimensional grid in the parameter space (b_1, b_2, b_3), so that the maximum of $\mathcal{L}$ could be found. The parameter b_4 is by definition $1 - b_2 - b_3$.
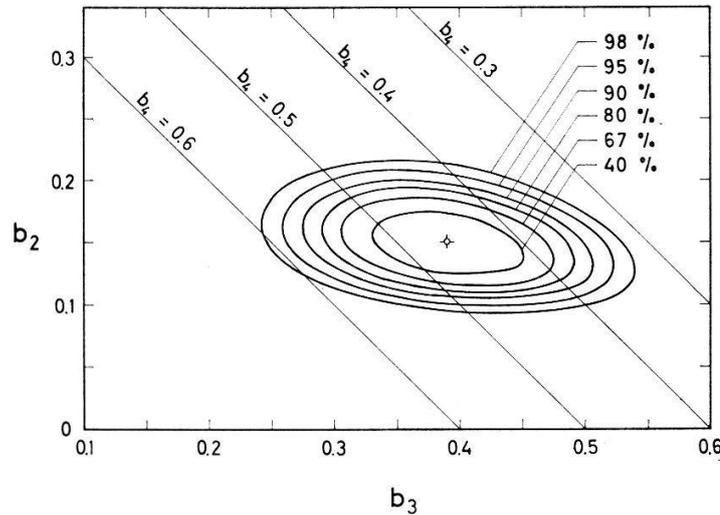
Fig. 14

Curves of equal likelihood in the $b_2 - b_3$ plane, for $b_1 = 0.67$. The curves are labelled with their respective confidence coefficients. The oblique straight lines at 45° represent the lines along which b_4 is constant.

The statistical errors were estimated from the likelihood function. The points in parameter space where $\mathcal{L}$ is down to a fixed fraction of its maximum value define the envelope of a closed region surrounding the maximum. The probability that the true values of the parameters are also contained somewhere inside this region may be given in the form of a confidence coefficient. For example the conditions that the likelihood function is down to $e^{-1.71}$, $e^{-3.13}$, or $e^{-4.86}$ of its maximum value define regions which have respectively 67%, 90%, or 98% as confidence coefficient. Figure 14 shows the contour lines of equal likelihood in the $b_2 - b_3$ plane, labelled with the corresponding confidence coefficients. For the 67% confidence interval we find:

$$\Delta b_{1 \text{ stat}} = \pm 0.06 \qquad \Delta b_{2 \text{ stat}} = \pm 0.03$$

$$\Delta b_{3 \text{ stat}} = \pm 0.07 \qquad \Delta b_{4 \text{ stat}} = \pm 0.07 .$$

As a check, five samples of Monte Carlo events were generated in the same numbers (440 events) and with the same branching ratios as those found for the experimental events (see Equation (23)). These samples were analysed with the maximum likelihood method, using classification probabilities obtained from the rest of the Monte Carlo events. The results are shown in Table 2, and indicate that the statistical errors we adopted are slightly overestimated.

Table 2

Branching ratios obtained by the maximum likelihood method in 5 samples of 440 Monte Carlo events each. The true values of the branching ratios b_1 to b_4 are given in the first column.

Generated	Sample 1	Sample 2	Sample 3	Sample 4	Sample 5
$b_1 = 0.67$	0.68	0.65	0.70	0.60	0.62
$b_2 = 0.15$	0.16	0.14	0.13	0.15	0.16
$b_3 = 0.39$	0.40	0.40	0.34	0.46	0.42
$b_4 = 0.46$	0.44	0.46	0.53	0.39	0.43

The errors due to events rejected in the course of the analysis can now be estimated from the arguments of §4.5. There we saw that 66 of the 116 events rejected for bad reconstruction contained the same proportions of different decay modes as the sample of 440 accepted K_2^0 decays, and that the 50 other badly-reconstructed events were mostly $\pi^\pm e^\mp \nu$ decays with some $\pi^\pm \mu^\mp \nu$ decays. Using our results of Equation (23) we can now estimate that this corresponds to between 7 and 13 $\pi^+ \pi^- \pi^0$ decays, between 20 and 60 $\pi^\pm \mu^\mp \nu$ decays, and between 25 and 70 $\pi^\pm e^\mp \nu$ decays.

Of the 48 well-reconstructed events which did not fit any of the ten K_2^0 decay hypotheses, 19 were compatible with decays of K_2^0's of very low momentum. These 19 events seemed to be in the same proportions as the branching ratios we obtain. To be safe, however, we estimate that the 48 events contain between 4 and 12 $\pi^+ \pi^- \pi^0$ decays, between 5 and 25 $\pi^\pm \mu^\mp \nu$ decays, and between 10 and 30 $\pi^\pm e^\mp \nu$ decays.

We therefore assume that in the total of 164 (= 116 + 48) discarded events there are between 11 and 25 $\pi^+ \pi^- \pi^0$ decays, between 25 and 85 $\pi^\pm \mu^\mp \nu$ decays, and between 35 and 100 $\pi^\pm e^\mp \nu$ decays. The greatest changes that could possibly be induced in the branching ratio estimates if these events were included in the sample of K_2^0 decays give the errors due to rejected events. The errors quoted in the final results are the

roots of the sum of squares of these errors and of the statistical ones. The final results are:

$$\frac{\text{No. of } \Lambda^0\text{-associated } K_2^0\text{'s}}{\text{Total no. of } K_2^0\text{'s}} = 0.67 \pm 0.10 \,,$$

$$\frac{\Gamma (K_2^0 \to \pi^+ \, \pi^- \, \pi^0)}{\Gamma (K_2^0 \to \text{all charged modes})} = \begin{array}{l} 0.15 + 0.03 \\ - 0.04 \,, \end{array}$$

$$\frac{\Gamma (K_2^0 \to \pi^\pm \, \mu^\mp \, \nu)}{\Gamma (K_2^0 \to \text{all charged modes})} = \begin{array}{l} 0.39 + 0.08 \\ - 0.10 \,, \end{array}$$

$$\frac{\Gamma (K_2^0 \to \pi^\pm \, e^\mp \, \nu)}{\Gamma (K_2^0 \to \text{all charged modes})} = \begin{array}{l} 0.46 + 0.08 \\ - 0.10 \,. \end{array} \tag{23}$$

The fraction of Λ^0-associated K_2^0's obtained in this estimate agrees well with the *a priori* value of 0.72 obtained in the K_2^0 spectrum calculations of Chapter III. The values of the branching ratios are in good agreement with those found by LUERS et al. [8], ADAIR and LEIPUNER [9], and VARDENGA et ai. [10].

6. Conclusions

6.1 *Discussion of the Method*

This method of obtaining the branching ratios is entirely based on the assumption that the classification probabilities obtained from the Monte Carlo events are also valid for the experimental ones. It is therefore important to take care that the artificial events resemble the real ones as closely as possible and also to check that any differences which may remain do not have a big influence on the classification probabilities.

The major source of possible discrepancies is the fact that the density of Monte Carlo events on the Dalitz plot may not be the same as the density of real events. We have already claimed that this will have no great effect because the outcome of the tests used in the tentative identification procedure are not sensitive to the point of the Dalitz plot where the event is situated. In the first five columns of Table 3 we compare the results obtained by assuming different types of interaction, and corre-

Table 3

Branching ratios obtained for the real events

	1	2	3	4	5	6	7
b_1	0.67	0.67	0.69	0.68	0.67	0.70	0.65
b_2	0.15	0.15	0.13	0.14	0.15	0.15	0.15
b_3	0.39	0.38	0.35	0.37	0.37	0.38	0.40
b_4	0.46	0.47	0.52	0.49	0.48	0.46	0.46

1) Assuming the spectrum of Equation (8) for the 3π decays and pure vector interaction with $f_2/f_V = 0$ for the leptonic events.
2) As 1), but with $f_2/f_V = 3.8$.
3) Assuming the spectrum of Equation (8) for the 3π decays and pure scalar interaction with a constant form factor for the leptonic events.
4) As 3), but with pure tensor interaction and a constant form factor for the leptonic events.
5) Assuming uniform density over phase space for all events.
6) As 1), but taking only the real events which lie within 10 cm of the axis of the chamber.
7) As 1), but taking only the real events more than 10 cm off axis.

spondingly different density distributions, for the K_2^0 decays. In Column 1 we give our quoted results, derived with the spectrum of Equation (8) for the $\pi^+ \pi^- \pi^0$ decays and with pure vector interaction and a constant form factor ratio $f_2/f_V = 0$ for the leptonic decays. Columns 2, 3, and 4 are derived with the same spectrum for the $\pi^+ \pi^- \pi^0$ events, but assume respectively for the leptonic events pure vector interaction with $f_2/f_V = 3.8$, pure scalar interaction with a constant form factor, and pure tensor interaction with a constant form factor. Column 5 assumes uniform density distribution for all types of decays.

Another discrepancy between the real and the artificial events is the fact that the apices of the Monte Carlo events are all situated along the longitudinal axis of the cloud chamber. To check that this has no appreciable effect we estimated the branching ratios within the subsample of real events which are less than 10 cm off the axis, and in the subsample of those outside this limit. The results are shown respectively in the sixth and seventh columns of Table 3.

The peak at 230 MeV/c in the K_2^0 momentum spectrum of the real events was not reproduced in the spectrum used for generating Monte Carlo events. Artificial events generated with a K_2^0 momentum smaller than 300 MeV/c indeed have a greater than average probability of being recognized by the tentative identification procedure as being Σ^0-associated, but their probabilities to appear as $\pi^+ \pi^- \pi^0$, $\pi^\pm \mu^\mp \nu$, or $\pi^\pm e^\mp \nu$ decays are the same as for the other events. The only effect of the lack of the peak at 230 MeV/c is thus to make the Monte Carlo events appear to contain less Σ^0-associated events. By comparison the real events may appear to contain slightly fewer Λ^0-associated events than they really do.

The external errors given by Equations (17) depend on the length L of the track. The Monte Carlo and the real events should therefore have the same average track length. The mean length of a track of an experimental event is 34 cm, that of an artificial event 39 cm. The small difference may be ascribed to the fact that the programme used for generating Monte Carlo events really follows each track right to the end, whereas human operators do not always measure a track to its extreme limit.

It must also be verified that the value $f_0 = 0.3$ mm, which was substituted into Equation (17), correctly represents the measurement error in the horizontal projection of the sagitta of a track. We have the following evidence that this is the case: the 'pulled quantities' δx_p are defined as:

$$\delta x_p = \frac{x_{\text{meas}} - x_{\text{fitted}}}{\sqrt{(\Delta x_{\text{meas}})^2 - (\Delta x_{\text{fitted}})^2}} \tag{24}$$

where x_{meas} can be the curvature, dip, or azimuthal angle of any measured track, and Δx_{meas} the initially estimated external error on x_{meas}; x_{fitted} and Δx_{fitted} are the values of the corresponding quantities after the GRIND fit. If the errors are correctly estimated, the distributions of the δx_p's which are obtained when the correct fit is attempted should be normal distributions with unit standard deviation [38]. This is indeed the case for the Monte Carlo events. For the real events, of course, we do not know which fit is the correct one. We therefore consider the distributions of the δx_p's obtained in the fit indicated by the tentative identification procedure. For the 66 real events tentatively identified as $\pi^+ \pi^- \pi^0$ decays, and in which the contamination by wrongly identified events is estimated at 20%, the δx_p's have standard deviations of

about 1.2. For the total sample of 440 real events, in which the contamination by wrongly identified events is about 50%, the standard deviations of the δx_p's are about 0.85. It is not surprising that they should be less than 1, because for the leptonic events the tentative identification procedure generally picks the interpretation for which the $x_{\text{meas}} - x_{\text{fitted}}$ are smallest. When the δx_p's of the ascribed fit (instead of those of the fit known to be correct) were plotted for the Monte Carlo events, the standard deviations were around 0.78.

6.2   Test of the $|\Delta I| = 1/2$ Rule

A test of the non-leptonic $|\Delta I| = 1/2$ rule which is free of any reference to absolute decay rates may be obtained by dividing Equation (7b) by Equation (7a). This leads to the relation:

$$\frac{\Gamma(K_2^0 \to \pi^0 \pi^0 \pi^0)}{\Gamma(K_2^0 \to \pi^+ \pi^- \pi^0)} = \frac{1}{2} \frac{1.565}{1.336} \left(1.295 \frac{\Gamma(K^+ \to \pi^+ \pi^+ \pi^-)}{\Gamma(K^+ \to \pi^+ \pi^0 \pi^0)} - 1\right).$$

Inserting the K^+ branching ratios obtained from the compilation of ROSENFELD et al. [16]:

$$\frac{\Gamma(K^+ \to \pi^+ \pi^+ \pi^-)}{\Gamma(K^+ \to \pi^+ \pi^0 \pi^0)} = \frac{5.5 \pm 0.1}{1.7 \pm 0.1} = 3.24 \pm 0.25$$

we obtain the prediction:

$$\frac{\Gamma(K_2^0 \to \pi^0 \pi^0 \pi^0)}{\Gamma(K_2^0 \to \pi^+ \pi^- \pi^0)} = 1.87 \pm 0.19$$

which has to be compared with the value obtained by combining our results with the weighted average of the results of ANIKINA et al. [44] and ALIKHANYAN et al. [45] for the branching ratio of $K_2^0 \to \pi^0 \pi^0 \pi^0$. The result is:

$$\frac{\Gamma(K_2^0 \to \pi^0 \pi^0 \pi^0)}{\Gamma(K_2^0 \to \pi^+ \pi^- \pi^0)} = \frac{0.24 \pm 0.06}{0.15 \pm 0.03} = 1.60 \pm 0.72.$$

Other checks of the non-leptonic and leptonic $|\Delta I| = 1/2$ rules may be obtained by using the data of ROSENFELD et al. [16] to calculate the absolute K^+ partial decay rates:

$$\Gamma(K^+ \to \pi^+ \pi^0 \pi^0) = (1.38 \pm 0.09)\ 10^6\ \text{sec}^{-1}$$

$$\Gamma(K^+ \to \pi^0 \mu^+ \nu) + \Gamma(K^+ \to \pi^0 e^+ \nu) = (6.67 \pm 0.36)\ 10^6\ \text{sec}^{-1}.$$

The prediction of the non-leptonic rule is then given by Equation (7a):

$$\Gamma(K_2^0 \to \pi^+ \pi^- \pi^0) = (2.84 \pm 0.19)\ 10^6\ \text{sec}^{-1}$$

and that of the leptonic rule by summing Equations (9a) and (9b):

$$\Gamma(K_2^0 \to \pi^\pm \mu^\mp \nu) + \Gamma(K_2^0 \to \pi^\pm e^\mp \nu) = (13.3 \pm 0.7)\ 10^6\ \text{sec}^{-1}.$$

These values have to be compared with those obtained by combining our branching ratios with the measurement of AUERBACH et al. [46]:

$$\Gamma(K_2^0 \to \text{all charged modes}) = (15.8 \pm 1.9)\ 10^6\ \text{sec}^{-1}.$$

This leads to the decay rates:

$$\Gamma(K_2^0 \to \pi^+ \pi^- \pi^0) = (2.37 \pm 0.76)\ 10^6\ \text{sec}^{-1}$$

$$\Gamma(K_2^0 \to \pi^\pm \mu^\mp \nu) + \Gamma(K_2^0 \to \pi^\pm e^\mp \nu) = (13.4 \pm 2.0)\ 10^6\ \text{sec}^{-1}.$$

In the case of the leptonic events the advantage of lumping the $\pi^\pm \mu^\mp \nu$ and $\pi^\pm e^\mp \nu$ decays together is to reduce the errors on our branching ratio for $K_2^0 \to$ leptonic modes to those produced by subtracting out the $\pi^+ \pi^- \pi^0$ contribution. By these tests both the non-leptonic and leptonic $| \Delta I | = 1/2$ rules are confirmed within the experimental errors.

Acknowledgements

References

[1] A. PAIS and M. GELL-MANN, Phys. Rev. *97*, 1387 (1955).

[2] M. BARDON, K. LANDE, L. M. LEDERMAN, and W. CHINOWSKY, Ann. Phys. (N.Y.) *5*, 156 (1958).

[3] J. H. CHRISTENSON, J. W. CRONIN, V. L. FITCH, and R. TURLAY, Phys. Rev. Lett. *13*, 138 (1964).

[4] A. ABASHIAN, R. J. ABRAMS, D. W. CARPENTER, G. P. FISHER, B. M. K. NEFKENS, and J. H. SMITH, Phys. Rev. Lett. *13*, 243 (1964).

[5] X. DE BOUARD, D. DEKKERS, B. JORDAN, R. MERMOD, T. R. WILLITTS, K. WINTER, P. SCHARFF, L. VALENTIN, M. VIVARGENT, and M. BOTT-BODENHAUSEN, Phys. Lett. *15*, 58 (1965).

[6] W. GALBRAITH, G. MANNING, A. E. TAYLOR, B. D. JONES, J. MALOS, A. ASTBURY, N. H. LIPMAN, and T. G. WALKER, Phys. Rev. Lett. *14*, 383 (1965).

[7] G. ALEXANDER, S. P. ALMEIDA, and F. S. CRAWFORD, Int. Conf. on High-Energy Physics at CERN, p. 448 (1962).

[8] D. LUERS, I. S. MITTRA, W. J. WILLIS, and S. S. YAMAMOTO, Phys. Rev. *133 B*, 1276 (1964).

[9] R. K. ADAIR and L. B. LEIPUNER, Phys. Lett. *12*, 67 (1964).

[10] G. P. VARDENGA, D. M. KOTLIAREVSKY, A. N. MESTVIRISHVILI, D. V. NEAGU, E. O. OKONOV, N. I. PETROV, V. A. RUSAKOV, and WU TSUN-FAN, Preprint P-1920, JINR, Dubna (1964).

[11] A. ASTIER, L. BLASKOVIC, M. M. DE COURREGES, B. EQUER, A. LLORET, P. RIVET, and J. SIAUD, Conf. Int. d'Aix-en-Provence sur les Particules Elementaires, p. 227 (1961).

[12] L. B. OKUN and E. P. SHABALIN, JETP *10*, 1252 (1960); E. P. SHABALIN, JETP *12*, 245 (1961).

[13] D. STERN, Phys. Rev. *128*, 389 (1962).

[14] B. AUBERT, L. BEHR, J. P. LOWSN, P. MITTNER, S. COLETTI, M. DI CORATO, and A. PULLIA, Sienna Int. Conf. on Elementary Particles, p. 20 (1963).

[15] F. R. EISLER, T. C. BACON, and H. W. K. HOPKINS, Preprint BNL 8239, Int. Conf. on High-Energy Physics at Dubna (1964).

[16] A. H. Rosenfeld, A. Barbaro-Galtieri, W. H. Barkas, P. L. Bastien, J. Kirz, and M. Roos, Rev. Mod. Phys. *36*, 977 (1964).

[17] R. H. Dalitz, Proc. Phys. Soc. London *A 69*, 527 (1956); R. H. Dalitz, Rev. Mod. Phys. *31*, 823 (1959).

[18] A. Pais and S. B. Treiman, Phys. Rev. *106*, 1106 (1957).

[19] R. F. Sawyer and K. C. Wali, Nuovo Cim. *17*, 938 (1960).

[20] S. Weinberg, Phys. Rev. Lett. *4*, 87 (1960); S. Weinberg, Phys. Rev. Lett. *4*, 585 (1960).

[21] I. Iu. Kobzarev and L. B. Okun, JETP *7*, 524 (1958).

[22] S. Okubo, R. E. Marshak, E. C. G. Sudarshan, W. B. Teutsch, and S. Weinberg, Phys. Rev. *112*, 665 (1958); S. Okubo, R. E. Marshak, and E. C. G. Sudarshan, Phys. Rev. Lett. *2*, 12 (1959).

[23] R. E. Behrends and A. Sirlin, Phys. Rev. *121*, 324 (1961).

[24] J. D. Jackson, Lectures at Brandeis University, *Elementary Particle Physics and Field Theory*, W. A. Benjamin, New York and Amsterdam, p. 263 (1962).

[25] R. Feynman and M. Gell-Mann, Phys. Rev. *109*, 193 (1958).

[26] N. Brene, L. Egardt, and B. Qvist, Nucl. Phys. *22*, 553 (1961).

[27] F. Zachariasen, Phys. Rev. *110*, 1481 (1958).

[28] A. Fujii and M. Kawaguchi, Phys. Rev. *113*, 1156 (1959).

[29] M. Barbier, J. D. Dowell, P. I. P. Kalmus, B. Leontic, A. Lundby, R. Meunier, G. Petrucci, L. Solinas, J. P. Stroot, and M. Szeptycka, Nucl. Instr. Meth. *20*, 66 (1963).

[30] C. Verkerk, Thesis, to be published.

[31] J. C. Brisson, J. Detoef, P. Falk-Vairant, L. van Rossum, G. Valladas, and Luke C. L. Yuan, Phys. Rev. Lett. *3*, 561 (1959).

[32] T. J. Devlin, B. C. Barish, W. N. Hess, V. Perez-Mendez, and J. Soloman, Phys. Rev. Lett. *4*, 242 (1960).

[33] L. Bertanza, P. L. Conolly, B. B. Culwick, F. R. Eisler, T. Morris, R. Palmer, A. Prodell, and N. P. Samios, Phys. Rev. Lett. *8*, 332 (1962).

[34] J. Steinberger, Int. Conf. on High-Energy Physics at CERN, p. 147 (1958).

[35] L. B. Leipuner and R. K. Adair, Phys. Rev. *109*, 1358 (1958).

[36] J. A. Anderson, F. S. Crawford, B. B. Crawford, R. L. Golden, L. J. Lloyd, G. W. Meisner, and L. R. Price, Int. Conf. on High-Energy Physics at CERN, p. 270 (1962).

[37] CERN Manual "THRESH"; G. R. Macleod, CERN Report 60-11 (unpublished); W. G. Moorhead, CERN Report 60-33 (unpublished).

[38] CERN Manual "GRIND"; R. Böck, CERN Report 60-30 (unpublished); R. Böck, CERN Report 61-29 (unpublished).

[39] M. Stearns, Phys. Rev. *76*, 836 (1949).

[40] P. Astbury, A. Michelini, C. Verkerk, F. Verkerk, W. Beusch, M. Pepin, and M. A. Pouchon, Phys. Lett. *18*, 175 (1965).

[41] G. Lynch, *Programme FAKE: Monte Carlo Simulation of Bubble Chamber Events*, UCRL-10335.

[42] CERN Manual "POST-GRIND".

[43] V. Bisi, G. Borreani, R. Cester, A. de Marco-Trabucco, M. I. Ferrero, C. M. Garelli, A. Marzari Chiesa, B. Quassiati, G. Rinaudo, M. Vigone, and A. Werbrouck, Nuovo Cim. *35*, 768 (1965).

[44] M. Kh. Anikina, M. S. Zhuravleva, D. M. Kotlyarevsky, Z. Sh. Mandzavidze, A. N. Mestvirishvili, D. V. Neagu, E. O. Okonov, N. I. Petrov, V. A. Rusakov, G. G. Takhtamyshev, L. V. Chkhaidze, and Wu Tsun-Fan, JETP *19*, 42 (1964).

[45] A. S. Sleksanyan, A. I. Alikhanyan, A. M. Gal'per, R. L. Kavalov, V. G. Kirillev-Ugryumov, L. P. Kotenko, L. A. Kuzin, E. P. Kyznetsov, and G. I. Merzon, JETP *19*, 1019 (1964).

[46] L. Auerbach, K. Lande, A. K. Mann, F. J. Sciulli, H. Uto, D. H. White, and K. K. Young, Phys. Rev. Lett. *14*, 192 (1965).